RSC Advances

PAPER

On the properties and atmospheric implication of amine-hydrated clusters†

Jiao Chen,[ab] Shuai Jiang,[a] Shou-Kui Miao,[a] Xiu-Qiu Peng,[a] Yan Ma,[a] Chun-Yu Wang,[a] Miao-Miao Zhang,[a] Yi-Rong Liu[a] and Wei Huang*[ab]

Amines have been recognized as important precursor species in the formation of new atmospheric particles. Although dimethylamine–water clusters have been the focus of a large number of theoretical studies during the last few years, some information regarding these clusters, such as the influence of temperature, the analysis of their weak interactions, and their Rayleigh scattering properties, is still lacking. In this study, the equilibrium geometric structures and thermodynamics of $(CH_3)_2NH(H_2O)_n$ ($n = 1$–6) clusters were systematically investigated using density functional theory (PW91PW91) coupled with the 6-311++G(3df,3pd) basis set. To determine the most stable isomer and the order of the different isomers, single-point calculations were executed using a two-point extrapolation method in conjunction with the complete basis set for all isomers. The optimized structures show that the addition of a fifth water molecule changes the most stable configuration from a quasi-planar ring structure to a cage-like configuration. Electron density analysis shows that the interactions of these complexes are mainly medium hydrogen bonds. The dependence on temperature of the conformational population and the Gibbs free energies of the $(CH_3)_2NH(H_2O)_n$ ($n = 1$–6) clusters were determined with respect to temperature (200–300 K). A weak dependence on temperature was found for the formation of $(CH_3)_2NH(H_2O)_n$ ($n = 1$–6) clusters. Dimethylamine–water clusters are favorable at low temperatures, but these clusters may be difficult to form because of the combined effect of Gibbs free energies with small negative values and the low relative concentration of dimethylamine in various atmospheric conditions, and this implies that dimethylamine–water clusters are difficult to form spontaneously in the atmosphere. Finally, the Rayleigh scattering properties of $(CH_3)_2NH(H_2O)_n$ ($n = 1$–6) have been investigated systematically for the first time.

1. Introduction

Atmospheric aerosols are solid or liquid particles suspended in the air, which play a key role in direct and indirect effects on the climate[1–5] by altering cloud properties and precipitation. The airborne ultrafine particles in these aerosols adversely affect public health.[6–8] The formation of new particles (NPF) has been observed in a wide range of locations and is estimated to be an important source of aerosol particles and cloud condensation nuclei. Recently, the formation of new particles has been observed;[4,9] however, investigating the initial stage of NPF remains a challenge, although state-of-the-art instruments[9] can measure ionic and neutral clusters. Understanding of the initial formation mechanisms of new particles is still deficient.[10–14]

Neutral binary sulfuric acid–water nucleation[4] and binary ion-induced nucleation[15] have been well studied and serve as an available point of comparison,[16,17] but they cannot explain new-particle formation events in the atmospheric boundary layer, which indicates that other species must participate in stabilizing sulfuric acid particles such as ions,[15,18,19] ammonia and amines,[20–27] organics,[28–33] and iodine oxides.[28] Quantum chemical calculations imply that nucleation with amines is significantly favorable over ammonia.[34–37] Several experimental studies have confirmed that ammonia and alkylamines strongly influence nucleation of sulfuric acid and water particles.[16,17,22,38–40] Moreover, recent field observations with gas-phase amines have corroborated that the presence of amines has a considerable effect on the formation of new particles.[41–44]

Dimethylamine (DMA) is the strongest and most common base in the atmosphere, and it can rapidly undergo acid–base reactions, which enhance neutral and ion-induced sulfuric acid–water nucleation.[36,40,41,45] Recently, reported studies have shown a correlation between the formation of new particles and the presence of DMA.[38,46–49] Experiments[38] using the CLOUD chamber at CERN confirmed that concentrations of DMA

[a] Laboratory of Atmospheric Physico-Chemistry, Anhui Institute of Optics & Fine Mechanics, Chinese Academy of Sciences, Hefei, Anhui 230031, China. E-mail: huangwei6@ustc.edu.cn

[b] School of Environmental Science & Optoelectronic Technology, University of Science and Technology of China, Hefei, Anhui 230026, China

† Electronic supplementary information (ESI) available. See DOI: 10.1039/c5ra11462d

exceeding three parts per trillion by volume were able to increase new-particle formation rates by more than 1000-fold compared to ammonia.

Hydrogen-bonding interactions are the driving forces for the formation of atmospheric molecular complexes, and their strength determines the thermodynamic stability of these complexes. Some quantum chemical studies of sulfuric acid, DMA and water have been performed,[34–36,50] but analysis of the weak attractions in the clusters, which are essential for their nucleation mechanism, is still absent. The theory of atoms in molecules (AIM), which was developed by Bader *et al.*,[51] is a valuable tool for understanding hydrogen bonds in molecular complexes. There are a number of studies dealing with the sulfuric acid–DMA–water system that show how DMA will not form clusters with water.[37,50,52,53] All this research was carried out at constant temperature and 1 atm. As we all know, the dependence on temperature of thermodynamic properties is a significant parameter for understanding how a specific nucleation mechanism plays a role in NPF. Furthermore, the climate is affected by aerosols directly *via* scattering the light from the sun.[54] Although the Rayleigh scattering properties of large particles are well understood, the Rayleigh scattering properties of clusters, especially at the molecular level, are still not known. Considering all these, AIM analysis, correlation with temperature and the investigation of Rayleigh scattering properties were performed for the first time in this study for clusters of $(CH_3)_2NH(H_2O)_{1-6}$.

This study includes some aspects as follows: (1) basin-hopping (BH) was coupled with density functional theory (DFT) and used to determine global and local minima by sampling the potential energy surface thoroughly; (2) single-point calculations were executed using a two-point extrapolation method in conjunction with the complete basis set for all isomers; (3) electron density analysis was performed to investigate the interactions of these complexes; (4) the dependence on temperature of the conformational population and the Gibbs free energies of the $(CH_3)_2NH(H_2O)_{1-6}$ clusters were investigated; and (5) the Rayleigh scattering properties of $(CH_3)_2NH(H_2O)_{1-6}$ have been investigated systematically for the first time.

2. Computational methods

As the number of water molecules increases, the number of isomers increases enormously, and the most stable conformers become obscure and not obvious. Therefore, searching large clusters by chemical intuition is very difficult. To overcome this problem, the BH algorithm[55–58] was employed, which has been successfully applied to atomic clusters.[58–63] To effectively search molecular clusters, the BH algorithm using a compressed sampling technique was improved in previous studies by applying the structures such as $(H_2O)_n$ ($n = 4–10$) clusters,[64] $CH_3NH_2–H_2O$ clusters,[65] $Cl^-(H_2O)$ clusters,[66,67] and $H_2SO_4–C_2H_2O_4–H_2O$ clusters.[68–71] The BH method includes two steps. First, a new structure is generated *via* the random displacement of atoms; then, the structure is optimized to a local minimum. Second, this local energy minimum is used as a criterion for

accepting the structure spaces that were initially generated with Boltzmann weight at a finite temperature. The initial geometries were obtained with the BH algorithm and PW91/DND implemented in the DMol³ software package[72] was employed in the DFT module coupled with BH. Then, the stable isomers within 10 kcal mol^{-1} of the stable global minimum were optimized *via* the PW91PW91/6-311++G(3df,3pd) method. For each stationary point, frequency calculations were carried out to ensure that there were no imaginary frequencies. The convergence standards used for optimization were the default settings in Gaussian09 software.[73] In the standard state of 1 atm pressure and 298 K, the binding energies, enthalpies, and Gibbs free energies were computed for all the selected clusters using the harmonic-oscillator and rigid-rotor approximations. Structural informations (bond lengths) were provided by Chemcraft 1.6 (http://www.chemcraftprog.com).

Previous studies have indicated that PW91PW91/6-311++G(3df,3pd) provides better performance for predicting the vibrational spectrum of oxalic acid than MP2/6-311++G(3df,3pd) or B3LYP/6-311++G(3df,3pd).[32,33,74,75] Moreover, it has been found that the PW91PW91 method well reproduces the MP2 and CCSD(T) results of the first hydration of sulfuric acid.[76] However, one of the main sources of error in quantum chemistry calculations is that the basis set is not sufficiently large or it is far from the complete basis set limit. Using PW91PW91 with a finite basis set for the calculation of the interaction energies of hydrogen-bonded systems encounters a problem called basis set superposition error (BSSE). To reduce this error and the calculation cost, extrapolation of the energy to the complete basis set (CBS)[77] limit was performed on the single-point energy calculated using the method of DF-MP2-F12. The CBS limit was estimated *via* a two-point extrapolation scheme.[78,79] The equations for the corresponding calculations are as follows:

$$E_{CBS}^{SCF} = E_N^{SCF} + B \times \exp(-AN) \tag{1}$$

$$E_{CBS}^{corr} = \frac{N^3 E_N^{corr} - (N-1)^3 E_{N-1}^{corr}}{N^3 - (N-1)^3}$$

$$E_{CBS}^{RI-MP2} = E_{CBS}^{SCF} + E_{CBS}^{corr}$$

where A and B are the fitting parameters and E_{CBS}^{SCF}, E_{CBS}^{corr} and E_{CBS}^{RI-MP2} are the SCF, correlation and total energies, respectively. All the calculations were performed using Molpro 2010.1[80] and the default convergence criteria were defined in Molpro 2010.1.

Although DFT methods can qualitatively describe geometries and vibrational frequencies, the weak interactions arising from dispersion forces are unable be accurately treated, which plays a moderately important role in hydrogen bonding. Two main pathways are provided to obtain accurate thermochemistry for hydrogen-bonded clusters. One method is to use DFT, which is sufficiently parameterized to replicate the binding energies of various benchmarking sets of weakly interacting clusters,

although the treatment of dispersion is inaccurate. Another alternative is to use correlated wave function-based methods such as MP perturbation theory or coupled-cluster methods. However, the computational cost of correlated wave function-based methods is generally orders of magnitude more than that of DFT methods. Herein, extrapolation is performed on energy values calculated by DF-MP2-F12 to reduce basis set superposition errors and basis set incompleteness errors. A study by Temelso et al.[81] showed that the convergence of the binding energy to the CBS is not monotonic, due to the incompleteness of the AVDE basis set resulting in an overestimation of the binding energy. Hill[82] demonstrated that the MP2-F12 method combined with the cc-pVnZ-F12 basis set produces results that are approximately equal to those from MP2-F12/aug-cc-pV(n + 1)Z. Aug sets include additional diffuse higher angular momentum functions, which lead to significantly more basis set superposition error than the cc-pVnZ-F12 basis set. Another important problem is the calculation of energies for larger clusters wherein the computational costs prohibit the use of large basis sets. Recent study illustrated that the binding energies from DF-MP2-F12/VQZ-F12 are close to the basis set limit.[83] To ensure accuracy without too high calculation cost, we selected DF-MP2-F12/cc-pVnZ-F12 (n = D, T) for the extrapolation scheme.

Two-point extrapolation by a conventional scheme (eqn (1)) was carried out by applying the cc-pVDZ-F12 and cc-pVTZ-F12 basis sets coupled with DF-MP2-F12 for calculating the SCF and correlation energies in this study. To obtain the fitting
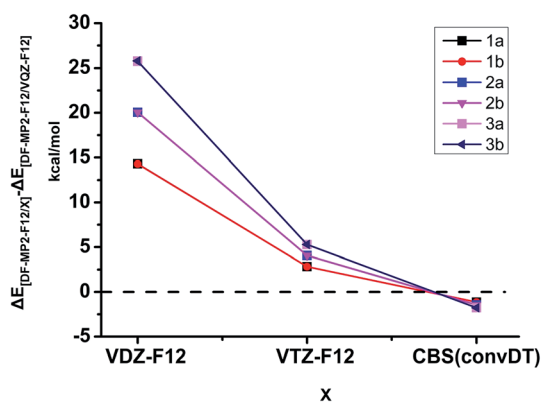
parameter A, which is a constant based on eqn (1), the binding energies for the six isomers of $(CH_3)_2NH(H_2O)_{n=1-3}$ were calculated at the DF-MP2-F12/cc-pVnZ-F12 (n = D, T, Q) level of theory. A three-point extrapolation was performed to fit the constant A, which is approximately equal to 1.48.

Fig. 1 shows that the convergence of the binding energy is monotonic; systematic convergence of the energies toward the CBS limit is again a feature of these basis sets. The two-point extrapolation scheme for the binding energy deviates from the benchmark DF-MP2-F12/VQZ-F12 with the difference increasing from 1.14 to 1.77 kcal mol^{-1} as the size of clusters grows. Thus, the deviation monotonically increases, which indicates that as the number of water molecules grows, the difference will increase correspondingly. For $(CH_3)_2NH(H_2O)_2$ and $(CH_3)_2NH(H_2O)_5$ clusters, the geometries of the most stable isomers optimized by the PW91PW91/6-311++G(3df,3pd) method were **2b** and **5d**, respectively. At the DF-MP2-F12/CBS// PW91PW91/6-311++G(3df,3pd) level, **2a** and **5a** were found to be the global minima. Furthermore, isomers with the same number of water molecules were arranged in order of increasing electronic energy. The difference in the calculated binding energies between CBS and DF-MP2-F12/cc-VTZ-F12 is several kcal mol^{-1} and with an increase in the size of the cluster, the errors in the Gibbs free energy for the same magnitude of binding energy will generate a significant effect on quantities, such as the abundance of clusters and nucleation rates, because they depend exponentially on barriers to nucleation.

Based on the global minima of $(CH_3)_2NH(H_2O)_n$ (n = 1–6) obtained in this study, the optical properties of the prenucleation clusters were evaluated. The light scattering intensities and isotropic mean polarizabilities $\bar{\alpha}$, as well as anisotropic polarizabilities $\Delta\alpha$, were calculated at the CAM-B3LYP/ aug-cc-pVDZ level of theory and the relevant computational methods are given in our earlier study.[66] The benchmark for the smallest clusters of H_2SO_4–NH_3–H_2O was determined by Elm et al.[84] They found that CAM-B3LYP/aug-cc-pVDZ gave a good balance between efficiency and accuracy and obtained good agreement with both experimental and CCSD(T) values of polarizability. In this article, to find an appropriate methodology for calculating the optical properties of DMA–H_2O clusters, five different DFT functionals with the aug-cc-pVDZ basis set were investigated. The results are shown in Table 1; by analyzing the results, CAM-B3LYP/aug-cc-pVDZ was confirmed to be a suitable method, which yielded good agreement with MP2 values of polarizability.

Fig. 1 Comparison of the differences between the binding energies for six isomers of $(CH_3)_2NH(H_2O)_{n=1,2,3}$ at the DF-MP2-F12/X and DF-MP2-F12/VQZ-F12 levels.

Table 1 Calculated isotropic mean polarizabilities of H_2O, CH_3NHCH_3, $(CH_3NHCH_3)(H_2O)$, and $(CH_3NHCH_3)(H_2O)_2$ using different DFT functionals with the aug-cc-pVDZ basis set

Functional	H_2O	CH_3NHCH_3	$(CH_3NHCH_3)(H_2O)$	$(CH_3NHCH_3)(H_2O)_2$
B3LYP	9.472	39.481	49.087	58.787
PW91PW91	10.051	41.143	56.648	61.809
M06-2X	8.893	38.351	47.072	56.437
ωB97x-D	9.185	38.431	47.553	56.925
CAM-B3LYP	9.326	38.477	47.781	57.283
MP2	9.301	38.486	47.699	57.320

3. Results and discussion

To understand the initial steps of the formation of new particles when DMA participates in forming new particles, we first performed quantum chemical calculations for $(CH_3)_2NH(H_2O)_n$ ($n = 1$–6) to search for the global minimum and several local minima. All the hydrated clusters with the same number of water molecules were arranged according to the binding energy with the ZPE correction from lowest to highest. The complexes were marked by n_a, n_b, n_c, etc., where n is the number of water molecules in the $(CH_3)_2NH(H_2O)_n$ clusters.

3.1 Structures

Monohydrates. In our search for the global and low-lying local minima of $(CH_3)_2NH(H_2O)$ clusters, the two structures shown in Fig. 2 were found to be the global minimum and local minimum in energy. According to Nadykto et al.,[35] isomer **1b** was reported to be the most stable isomer. High-level calculation at the DF-MP2-F12/CBS//PW91PW91/6-311++G(3df,3pd) level showed that **1a** was the lowest structure.

Dihydrates. In our search for the global minimum of the $(CH_3)_2NH(H_2O)_2$ cluster, the ground-state geometry of isomer **2b** shown in Fig. 2 was optimized at the PW91PW91/6-311++G(3df,3pd) level, which agrees with the previous result.[35] We calibrated the single-point energy at the DF-MP2-F12/CBS//PW91PW91/6-311++G(3df,3pd) level. Configuration **2b** is the

structure with the second lowest energy, which is higher in energy by 0.24 kcal mol^{-1} than **2a**.

Trihydrates. Eight isomers were taken into account (in Fig. 2). According to the arrangement, there are two types of pattern in the cyclic forms. The three isomers with lowest energy (**3a**, **3b** and **3c**) are similar and have four-membered ring structures with four HBs. The atoms forming the HB network nearly lie in the same plane, and the difference in the orientation of the three isomers is due to the free hydrogen atoms. Therefore, the binding energies are very similar. For the other five isomers, three water molecules form a coplanar three-membered ring structure, except for the free hydrogen atoms. The orientation of the free hydrogen atoms and the three-membered ring gives rise to a difference in the structure and binding energies. For the first type, the computed binding energies with the zero-point energy correction for each structure exhibit small gaps; compared with the most stable structure, the differences in energy are 0.12 kcal mol^{-1} and 0.39 kcal mol^{-1}. In contrast, a wide gap exists between the two types on the binding energies, ranging from 2.79 kcal mol^{-1} to 3.80 kcal mol^{-1}. This gap means that the four-membered ring structure is more stable than the three-membered ring structure. The structure of **3a** is similar to the global minimum of the $(H_2O)_4$ cluster.[85]

Tetrahydrates. The most stable configuration (**4a**) for $(CH_3)_2NH(H_2O)_4$ clusters is a ring structure with five H-bonds, which is similar to the cluster of $(H_2O)_5$.[85] The HB length of
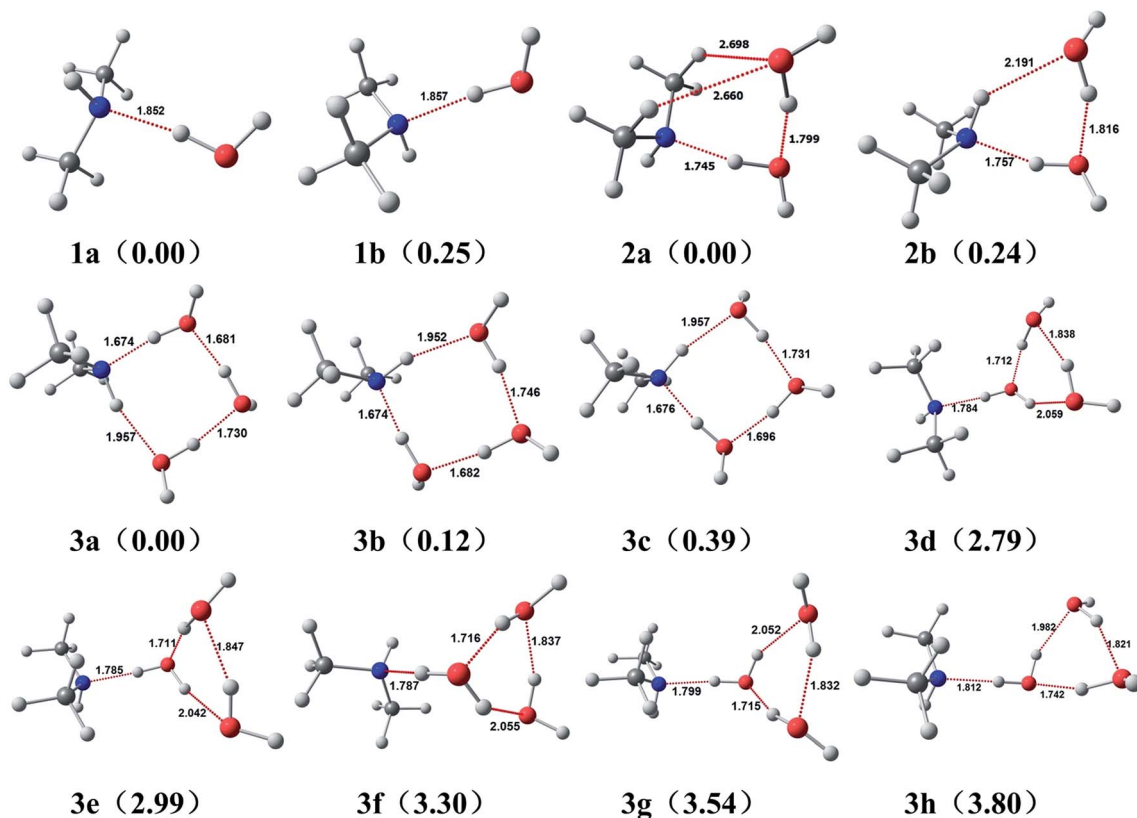

Fig. 2 Global minimum and local minima for $(CH_3)_2NH(H_2O)_{n=1-3}$ optimized at the PW91PW91/6-311++G(3df,3pd) level. The relative energies (kcal mol^{-1}) with respect to the most stable structure are given in parentheses.

N–H⋯O is 1.909 Å, which is weaker than the others (1.643 Å, 1.644 Å, 1.667 Å, and 1.702 Å). Interestingly, with a change in the orientation of the free hydrogen, the configurations labeled **4b** and **4e** became distorted and are no longer planar. The clusters change from planar to contorted planar to minimize repulsions from the adjacent hydrogens. For **4h** and **4i**, four water molecules form a four-membered ring with similar features to the trihydrates. In addition to the single-ring structures, four bicyclic structures (**4d**, **4f**, **4g** and **4j**) are observed. Detailed informations about these structures are shown in Fig. 3.

Pentahydrates. For the case of the $(CH_3)_2NH(H_2O)_5$ cluster in Fig. 4, eighteen low-lying isomers within 4 kcal mol^{-1} were selected. Compared with the trihydrate and tetrahydrate clusters, the fifth water molecule produces a significant change in the most stable structure, changing it from a planar ring to a three-dimensional form. For the pentahydrate clusters, the most stable structure is a prism structure lacking one side with eight H-bonds, whereas it is a complete prism structure for the $(H_2O)_6$ cluster.[85] The geometry of **5b** is closest to that of **5a**, although its binding energy lies higher by 0.85 kcal mol^{-1}. The orientation of the free hydrogen and the relative orientation between DMA and hydrated ring structures make the conformation different. The binding energies of these similar isomers display small gaps that are within a few kcal mol^{-1}. Many configurations are derived from $(CH_3)_2NH(H_2O)_4$ clusters. For instance, **5i** is a derivative of the existing structure **4h** with the addition of H_2O and minor rearrangements to the existing
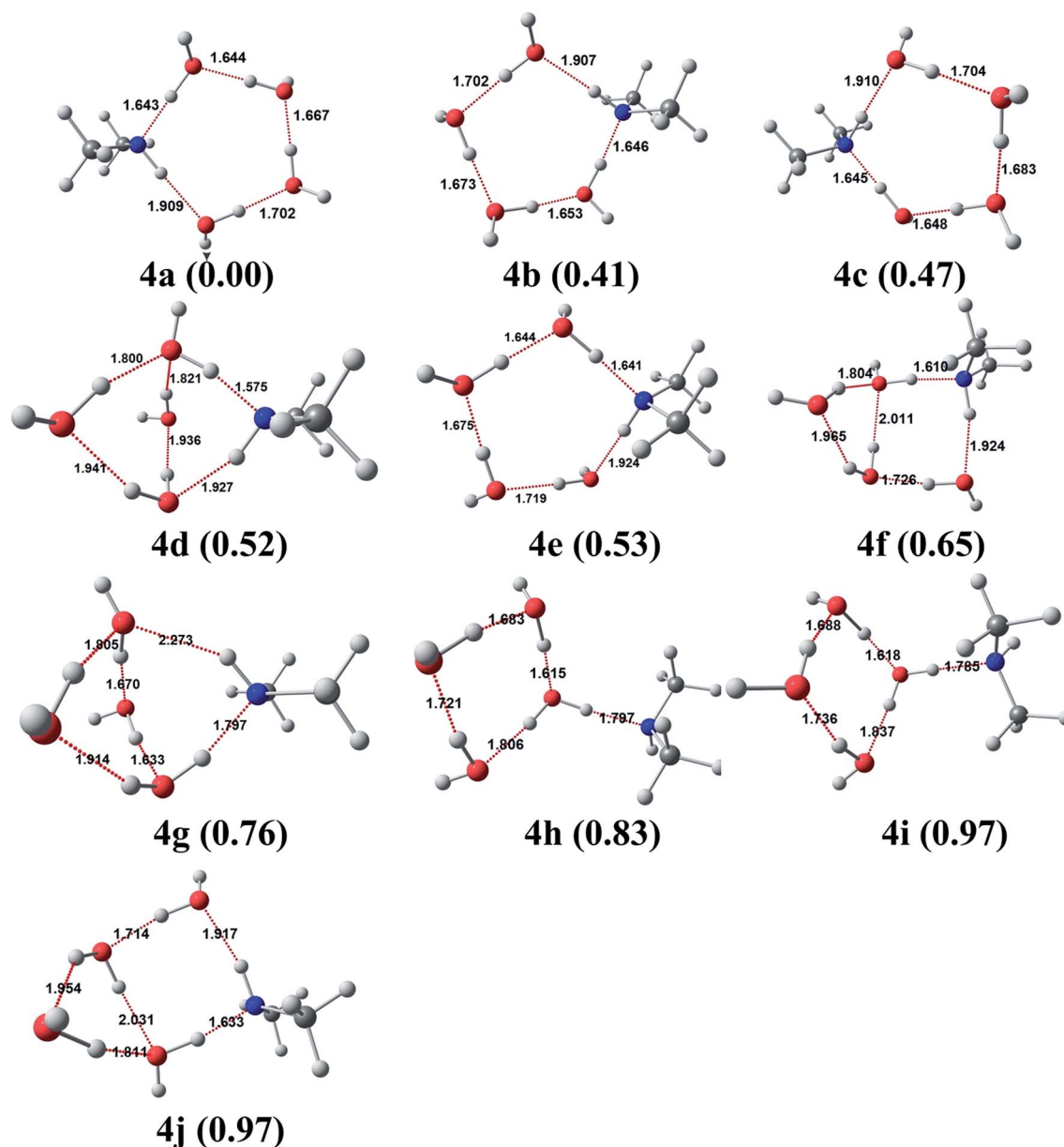

Fig. 3 Global minimum and local minima for $(CH_3)_2NH(H_2O)_4$ optimized at the PW91PW91/6-311++G(3df,3pd) level. The relative energies (kcal mol^{-1}) with respect to the most stable structure are given in parentheses.

network of HBs. Similarly, **5e** is a derivative of **4d**. The frequency calculation, which was performed on **5k** shows that it has one imaginary frequency of 3.15. This imaginary frequency is so small that the geometry can be considered as a local-minimum structure.

Hexahydrates. Among the stable isomers of the $(CH_3)_2$-$NH(H_2O)_6$ cluster in Fig. 5, isomer **6a** is the structure with lowest energy and was derived from isomer **5a** with one water molecule inserted into the existing HB network and then forming a non-planar four-membered ring. The second most stable structure (**6b**) has a slightly distorted cube-like structure with a corner missing and is similar to the most stable $(H_2O)_7$

cluster.[85] Although structures **6b** and **6d** are similar to **6a**, which are derived from **5a**, a considerable alteration was generated, because the sixth water molecule is located at a different position compared to isomer **5a**. Our calculations of the binding energies for **6a** and **6b** without the ZPE correction (in Table 3) show that **6a** lies slightly higher than **6b** by 0.27 kcal mol^{-1}. Due to the formation of HBs between amino hydrogen atoms and the oxygen atoms of water molecules, **6c**, **6e** and **6h** are all polycyclic structures with nine H-bonds. When the amino hydrogen atom is free, different types of polycyclic structures (**6i**, **6k** and **6l**) are composed of six water molecules. In addition
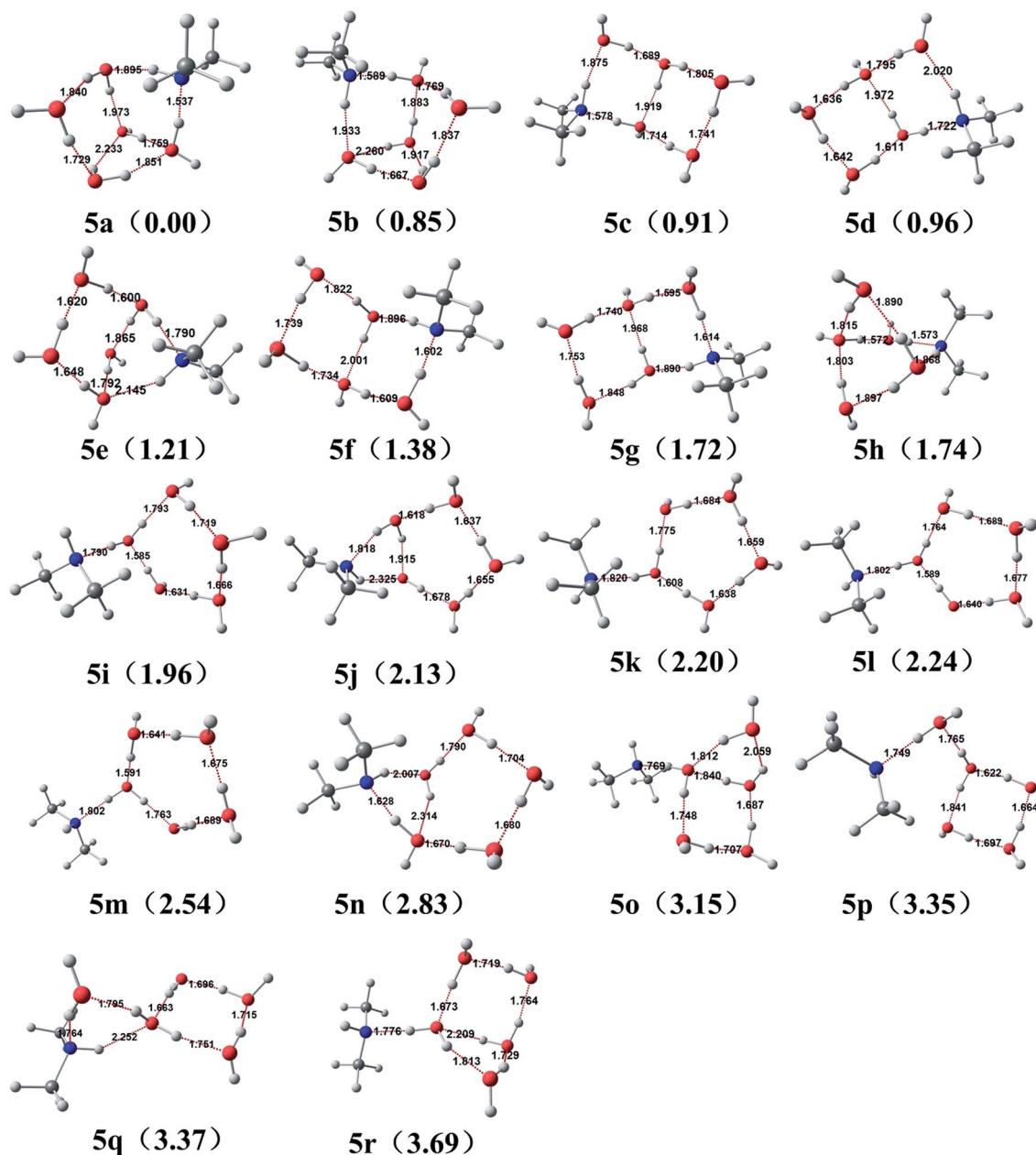

Fig. 4 Global minimum and local minima for $(CH_3)_2NH(H_2O)_5$ optimized at the PW91PW91/6-311++G(3df,3pd) level. The relative energies (kcal mol^{-1}) with respect to the most stable structure are given in parentheses.

Fig. 5 Global minimum and local minima for $(CH_3)_2NH(H_2O)_6$ optimized at the PW91PW91/6-311++G(3df,3pd) level. The relative energies (kcal mol^{-1}) with respect to the most stable structure are given in parentheses.
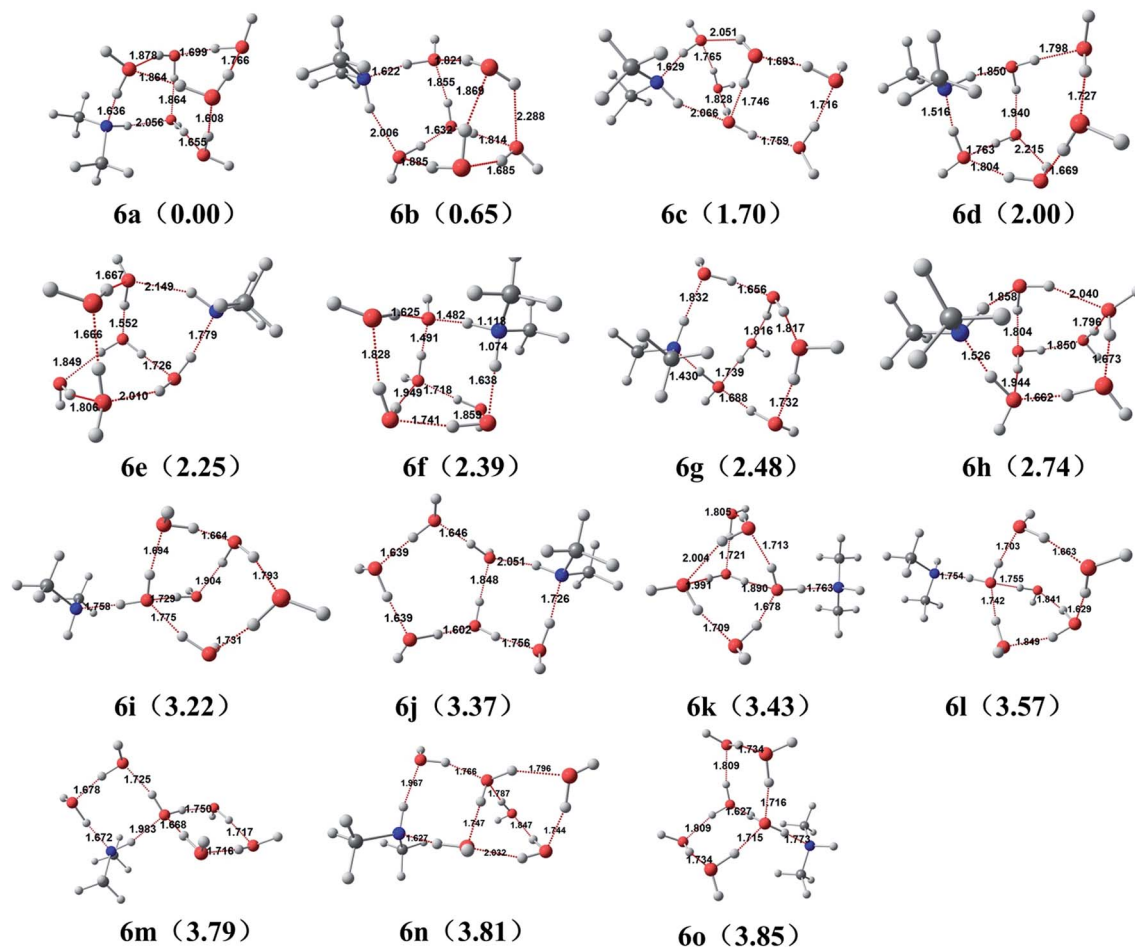
to the polycyclic structures, there are many bicyclic structures such as **6j** with eight H-bonds.

3.2 Electron density analysis

As intermolecular interaction distances are just below the sum of the van der Waals radii of atoms naturally, they cannot be used to determine the strength of hydrogen bonds and the nature of any possible bonding between methyl groups and water molecules, or even for revealing steric interactions. Therefore, AIM theory provided by topological analysis of the electron density was performed here to deepen understanding of the intermolecular hydrogen bonding of the most stable conformations. The basis of the topological parameters at the bond critical points (BCPs) was calculated based on Bader's atoms in molecules theory.[51] Some representative parameters for this type of interaction were chosen such as the electron density ρ, the Laplacian of the electron density $\nabla^2\rho$, the kinetic electron energy density G, the potential density V, the electron energy density H, and the value of $G/|V|$ at the bond critical point. The values of $\nabla^2\rho$ and H indicate the nature of the interaction and a negative value of $\nabla^2\rho$ shows that there is a shared interaction as in a covalent bond, whereas a positive

value indicates closed-shell system interactions such as HB and van der Waals forces. Furthermore, the energy density has proved to be a more appropriate and sensible criterion than $\nabla^2\rho$ to characterize the strength of hydrogen bonds. Thus, both $\nabla^2\rho$ and $H > 0$ represent weak HB, $\nabla^2\rho > 0$ and $H < 0$ indicate medium HB, whereas both $\nabla^2\rho$ and $H < 0$ show strong HB. Moreover, $G/|V|$ taken as the ratio between a positive value of G and a negative value of V may indicate bonds corresponding to covalent or non-covalent interaction. Thus, if $G/|V|$ is greater than 1, the interaction has the character of a closed-shell non-covalent interaction. If the ratio is between 0.5 and 1, the interaction is partly covalent in nature and if it is less than 0.5, the interaction is a shared covalent interaction.

From Table S1,† it is observed that the values of $\nabla^2\rho$ of the most stable conformations at the BCPs are all positive except for O5–H14···O2 of isomer **6a**. All the O–H···N linkages display medium HBs with $H < 0$. And the corresponding values of $\nabla^2\rho$ decrease with an increase in the number of water molecules up to five in the range of 0.0735–0.0051 a.u., whereas $\nabla^2\rho$ exhibits a large step increase for **6a**. For isomer **2a**, C–H6···O2 and C–H7···O2 are both non-covalent because the values of $G/|V|$ are greater than 1. In the cases of **3a** and **6a**, the HBs

Paper

Table 2 Comparison of changes at the DF-MP2-F12/CBS level in terms of ΔE (kcal mol^{-1}), ΔE + ZPE (kcal mol^{-1}), ΔH (kcal mol^{-1}), and ΔG (kcal mol^{-1}) associated with formation of $(CH_3)_2NH(H_2O)_{n=1-4}$. The zero-point energy, thermal correction to enthalpy and Gibbs free energy were calculated from vibrational analysis at the PW91PW91/6-311++G(3df,3pd) level (1 atm, 298 K)

Reaction	Isomer	ΔE	ΔE + ZPE	ΔH	ΔG
$(CH_3)_2NH + H_2O \leftrightarrow (CH_3)_2NH \cdot H_2O$	**1a**	-7.72	-5.63	-5.99	1.60
	1b	-7.45	-5.43	-5.74	1.46
$(CH_3)_2NH \cdot H_2O + H_2O \leftrightarrow$	**2a**	-9.04	-6.64	-7.41	2.25
$(CH_3)_2NH \cdot 2H_2O$	**2b**	-8.95	-6.53	-7.36	2.49
$(CH_3)_2NH \cdot 2H_2O + H_2O \leftrightarrow$	**3a**	-10.48	-8.07	-9.04	1.02
$(CH_3)_2NH \cdot 3H_2O$	**3b**	-10.15	-7.95	-8.78	0.67
	3c	-10.02	-7.68	-8.61	1.25
	3d	-7.97	-5.28	-6.14	2.93
	3e	-7.76	-5.08	-5.94	3.07
	3f	-7.4	-4.77	-5.58	2.51
	3g	-7.11	-4.53	-5.31	2.81
	3h	-6.92	-4.27	-5.07	3.28
$(CH_3)_2NH \cdot 3H_2O + H_2O \leftrightarrow$	**4a**	-8.69	-6.64	-7.26	1.42
$(CH_3)_2NH \cdot 4H_2O$	**4b**	-8.17	-6.23	-6.76	1.65
	4c	-8.08	-6.16	-6.7	1.44
	4d	-8.41	-6.11	-6.85	3.11
	4e	-8.13	-6.1	-6.7	1.77
	4f	-8.16	-5.98	-6.56	2.75
	4g	-8.62	-5.88	-6.76	3.14
	4h	-8.52	-5.81	-6.61	1.14
	4i	-8.34	-5.67	-6.48	2.15
	4j	-7.81	-5.66	-6.17	2.72

formed between an amino hydrogen atom and the oxygen atom of a water molecule are both non-covalent. For **4a**, all the HBs are medium HBs. For **5a**, except for the HBs in C–H13···O3, O2–H11···O6 and O4–H15···O6, the other HBs in this structure display the characteristics of medium HBs. As the number of water molecules increases to six, a strong HB in O5–H14···O2 was observed.

The non-covalent interactions (NCI) analysis method, which is derived from the correlation between the reduced density gradient and the electron density, has been studied by Yang et al.[86,87] The reduced density gradient

$$s = \frac{1}{2(3\pi^2)^{1/3}} \frac{\nabla \rho}{\rho^{4/3}}$$

is a fundamental dimensionless quantity in DFT that is presented to describe the deviation from a homogeneous electron distribution.[86] To a certain extent, NCI analysis can be regarded as an extension of AIM.[87] Not only can the location of pairwise atoms that are connected along the bond path be identified, the properties around BCPs can also be visualized using NCI. The reduced density gradient is able to be used to confirm covalent interactions and non-covalent interactions in real space.[88]

Fig. 6 shows the reduced gradient isosurfaces ($s = 0.5$ a.u.) using the Multiwfn program[89] and VMD program.[90] The green to blue-colored regions of the binding isosurface indicate that the HB interaction is becoming stronger. HBs that consist of ammonia nitrogens and hydrogen atoms of water molecules are the strongest HBs for every conformation and their strength becomes greater as the number of water molecules increases. At the same time, steric hindrance cannot be neglected because of the two methyl groups. Furthermore, repulsions located at the

center of an H-bond ring are very weak and the more H-bonds form a ring, the weaker becomes the repulsion. However, there is medium hydrogen-bonding interaction building up between DMA and water molecules, which is not substantial enough to overcome the energy barrier for the reaction of hydration spontaneously in the standard state of 1 atm pressure and 298 K.

3.3 Thermodynamics of $(CH_3)_2NH(H_2O)_n$ formation

The binding energies ΔE (kcal mol^{-1}) of the clusters were calculated using the following equation. The ZPE-corrected binding energies ΔE + ZPE (kcal mol^{-1}), interaction enthalpies ΔH (kcal mol^{-1}) and changes in Gibbs free energy ΔG (kcal mol^{-1}) were calculated in the same way:

$$\Delta E_{(CH_3)_2NH(H_2O)_n} = E_{(CH_3)_2NH(H_2O)_n} - E_{(CH_3)_2NH(H_2O)_{n-1}} - E_{H_2O}$$

Tables 2 and 3 show the thermodynamics of the most stable configurations at the DF-MP2-F12/CBS level of theory upon adding a water monomer to the most stable $(CH_3)_2NH(H_2O)_{n-1}$ cluster to form $(CH_3)_2NH(H_2O)_n$ clusters. Furthermore, ΔE (kcal mol^{-1}), ΔE + ZPE (kcal mol^{-1}), ΔH (kcal mol^{-1}) and ΔG (kcal mol^{-1}) were calculated.

Fig. 7 presents how the binding energy, enthalpy and Gibbs free energy of the global minimum change with an increase in the cluster size. The change in the binding energy is non-monotonic, and the binding energy with the ZPE correction ranges from -5.63 to -10.88 kcal mol^{-1} during the stepwise addition of water monomers. As one to three water molecules are added, the binding energy gradually becomes more negative

Table 3 Comparison of changes at the DF-MP2-F12/CBS level in terms of ΔE (kcal mol^{-1}), ΔE + ZPE (kcal mol^{-1}), ΔH (kcal mol^{-1}), and ΔG (kcal mol^{-1}) associated with formation of $(CH_3)_2NH(H_2O)_{n=5-6}$. The zero-point energy, thermal correction to enthalpy and Gibbs free energy were calculated from vibrational analysis at the PW91PW91/6-311++G(3df,3pd) level

Reaction	Isomer	ΔE	ΔE + ZPE	ΔH	ΔG
$(CH_3)_2NH \cdot 4H_2O + H_2O \leftrightarrow$	**5a**	−10.36	−7.68	−8.66	2.64
$(CH_3)_2NH \cdot 5H_2O$	**5b**	−9.91	−6.83	−7.92	3.35
	5c	−9.41	−6.77	−7.69	2.67
	5d	−9.51	−6.72	−7.62	2.18
	5e	−9.31	−6.47	−7.44	2.87
	5f	−8.91	−6.3	−7.22	2.94
	5g	−8.53	−5.96	−6.85	3.26
	5h	−8.38	−5.94	−6.84	3.32
	5i	−8.54	−5.72	−6.62	2.4
	5j	−8.28	−5.55	−6.36	2.68
	5k	−8.25	−5.48	−6.88	3.89
	5l	−8.23	−5.44	−6.27	2.01
	5m	−7.94	−5.14	−5.96	2.36
	5n	−7.24	−4.85	−5.52	3.85
	5o	−7.58	−4.54	−5.27	2.79
	5p	−7.3	−4.34	−5.21	3.82
	5q	−7.26	−4.31	−5.14	3.55
	5r	−7.22	−3.99	−4.85	3.79
$(CH_3)_2NH \cdot 5H_2O + H_2O \leftrightarrow$	**6a**	−11.64	−10.88	−9.64	0.80
$(CH_3)_2NH \cdot 6H_2O$	**6b**	−11.37	−10.23	−9.09	1.58
	6c	−9.68	−9.18	−7.68	1.52
	6d	−8.74	−8.88	−7.26	2.18
	6e	−9.40	−8.63	−7.33	2.55
	6f	−8.93	−8.48	−7.76	4.48
	6g	−7.56	−8.40	−6.78	2.59
	6h	−8.25	−8.14	−6.67	3.16
	6i	−8.54	−7.66	−6.12	1.85
	6j	−7.61	−7.51	−5.83	1.46
	6k	−8.44	−7.45	−5.98	2.20
	6l	−8.01	−7.30	−5.75	2.15
	6m	−7.17	−7.08	−5.33	1.66
	6n	−7.39	−7.07	−5.38	2.98
	6o	−7.71	−7.02	−5.44	2.31

because new ring hydrogen bonds are formed. In the case of the $(CH_3)_2NH(H_2O)_4$ cluster, this tendency is reversed and there appears to be a maximum energy rise in the stepwise hydration. By adding the fifth water molecule, the relative stabilization is increased as the conformation changes from 2-dimensional to 3-dimensional. In the case of the $(CH_3)_2NH(H_2O)_6$ cluster, the binding energy rapidly decreases and there appears to be an energy minima in the stepwise hydration. This discrepancy resulted from the differences between the most stable conformations. The results showed that the stability of the clusters varies, and the discrepancies depend on (a) the number of H-bonds, (b) the network of H-bonds, (c) the configuration of the isomers (*e.g.* quasi-planar, distortion-planar and three-dimensional), (d) whether the amino nitrogen atom is involved in hydrogen bonding and (e) the orientation of free hydrogen atoms. These factors determine which isomer is the global minimum. The non-monotonic change in enthalpy is similar to the variation of binding energy with the ZPE correction.

The non-monotonic change in ΔG with the addition of each successive water molecule (Fig. 7) is different from the change in the binding energy. For $(CH_3)_2NH(H_2O)_3$, the most stable structure corresponds to ΔG being minimized and the maximum Gibbs energy of interaction is obtained when the fifth water molecule is added. Tables 2 and 3 show that all the reactions involving the addition of water monomers are slightly exothermic. Due to the types of HB networks and the length of HBs, there is no absolute correlation between the contribution of enthalpy and the number of hydrogen bonds. The addition of more water molecules results in a cage of more H-bonds and in most cases the structures with lowest free energy have the fewest H-bonds because of entropic cost. Up to this point, clusters with up to six water molecules have been discussed. Thermodynamically, the formation of these structures is clearly unfavorable. The magic number of water molecules that is thermodynamically favored remains unknown. Because of the positive free energy, the equilibrium hydrate distributions are very small and these clusters cannot form spontaneously at 298 K and 1 atm. However, this study can act as a reference for the study of ternary nucleation systems containing DMA, sulfuric acid and water molecules. The study by Xu *et al.*[33] shows that, although the formation of DMA hydrates is not favorable, the formation of H_2SO_4–DMA–$(H_2O)_n$ clusters is more favorable *via* the collision between H_2SO_4 and
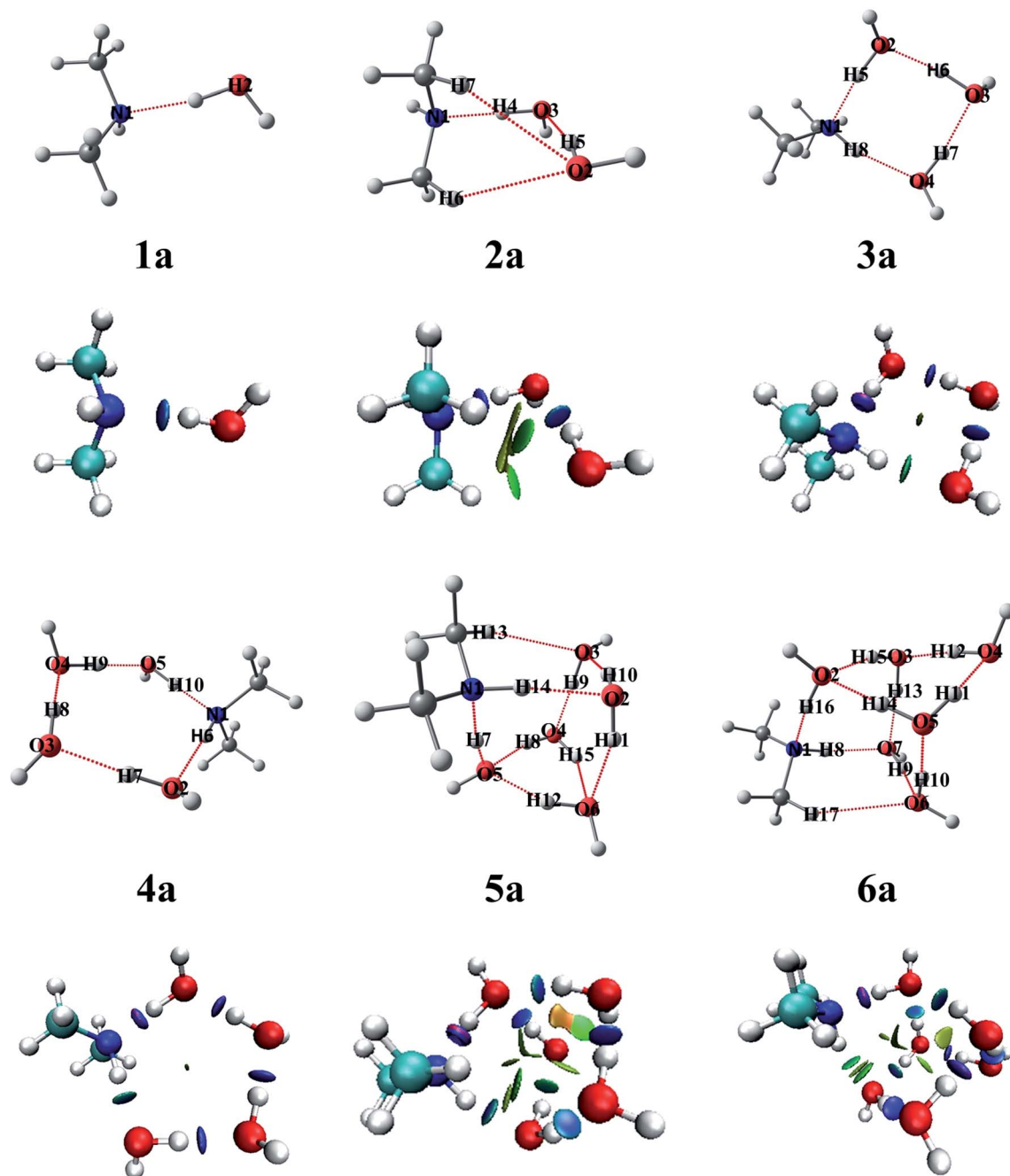
Fig. 6 Lowest-energy structures and isosurfaces ($s = 0.5$ a.u.) of the $(CH_3)_2NH(H_2O)_6$ clusters at the PW91PW91/6-311++G(3df,3pd) level.

DMA–$(H_2O)_n$ clusters than between H_2SO_4–$(H_2O)_n$ clusters, DMA, and more water molecules.

3.4 Temperature dependence of the conformational population and Gibbs free energy

The contribution from the global minimum is important for the ensemble of energetically accessible conformations because it has the largest population. However, as the cluster systems become larger and the configurations more complex, the difference in energy between the global minimum and low local minima becomes smaller due to the flexible HB networks.

These results indicate that the local minima might be as significant as those with larger weighting. The dependence on temperature of the thermodynamics is also an important parameter that could change the order of stability of the global minimum and the local minimum as well as the weighting of the isomers. Thus, the effects of temperature on the contributions of lower local minima were investigated in this study, which could give insight into the relative stabilities of the different isomers. The relevant computational methods are given in our earlier study.[70]
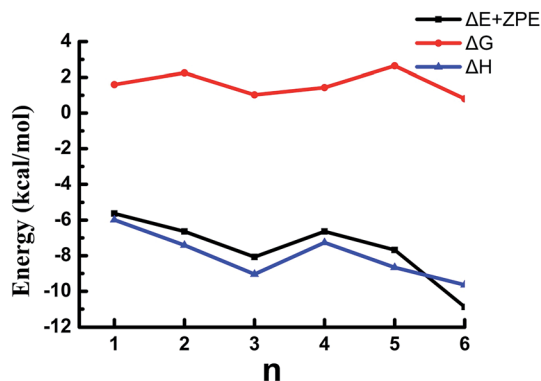
Fig. 7 Comparison of the binding energies, enthalpies and Gibbs free energies of the global minimum for the stepwise hydration of DMA at the DF-MP2-F12/CBS (limit DZ, TZ) level [$(CH_3)_2NH(H_2O)_{n-1}$ + H_2O → $(CH_3)_2NH(H_2O)_n$].

The variation of the population of the isomers *versus* the temperature is presented in Fig. 8. For $(CH_3)_2NH(H_2O)$, the proportion of the global minimum of **1a** is less than that of isomer **1b**, and as the temperature increases, the weighting of **1b** increases monotonically. The difference between the two isomers gradually increases. Fig. 8a shows the results for $(CH_3)_2NH(H_2O)_2$ clusters. The weighting of the global minimum of **2a** decreases slightly from 212.6 to 249.9 K, reaching a maximum of 62.92% and then decreasing to a minimum of 60.01% at 298.15 K. In the case when $n = 3$, **3b** has the largest proportion and this increases slowly for the entire time. Moreover, the total population of **3a**, **3b** and **3c** is approximately 100%, which indicates that a cyclic structure with four H-bonds is the most stable structure for trihydrates. Fig. 8c presents the conformational population of isomers for $n = 4$. The populations of the local minima increase, whereas that of the global minimum decreases monotonically as the temperature increases. A strong entropy effect can be observed in **4h** for the population with the largest entropy. For the case when $n = 5$, given in Fig. 8d, our results predict a monotonic increase for **5i**, **5l**, and **5m** with respect to temperature. The growth rate of **5l** is clearly higher than that of the other isomers and **5l** has the largest proportion above a temperature of 259.3 K, which indicates that planar structures play a leading role at high temperatures. The populations of **5d** and **5a** fall slightly and significantly, respectively. However, **5d** is more heavily populated than **5a** as the temperature increases. The weightings for other isomers almost remain constant and their proportions are so small as to be negligible. In the case of $n = 6$, the weighting of the global minimum is the largest among all the isomers in the temperature range from 212.6 to 298.15 K. Similarly, the population of **6a** decreased dramatically from 72.44% to 35.39%. The local minima, except for isomer **6b**, increase as the temperature increases. In conclusion, the weightings of the global minima and local minima change as the temperature increases. The effects of temperature could contribute to the alteration of the order of stability of the isomers.

The dependence on temperature of Gibbs free energy for the formation of $(CH_3)_2NH(H_2O)_{n=1-6}$ clusters with respect to different temperatures (200–300 K) was investigated. Fig. 9 shows the minimum thermodynamics for stepwise hydration of $(CH_3)_2NH(H_2O)_{n=1-6}$. There is a strong dependence on temperature for the formation of $(CH_3)_2NH(H_2O)_{n=1-6}$ clusters. The lowest free energy shifts from $n = 6$ below 223.7 K to $n = 3$ around 230 K. As the temperature falls below 223.7 K, the stepwise addition from one to six water molecules into DMA clusters is favorable. As the temperature increases, the clusters become less favorable and as the temperature reach 298.15 K, all the clusters become unfavorable. According to Kim *et al.*,[91] it is easy to change the stabilities of clusters containing multiple hydrogen bonds when the temperature rises, which is a result of the entropy effect. Although hydrated DMA clusters are favorable at low temperatures, these clusters could not form because of the combined effect of Gibbs free energies with small negative values and the low relative concentration of DMA in various atmospheric conditions.

3.5 Optical properties

Aerosols weaken light by absorbing and scattering and extinction properties have a great effect on atmospheric visibility and radiative forcing.[92,93] Rayleigh scattering is the principal form of scattering for molecules, clusters, and small particles with diameters much smaller than the wavelength of the light. Although the Rayleigh scattering properties of large particles are well understood, the Rayleigh scattering properties of clusters, especially at the molecular level, are still not known. In this study, the Rayleigh scattering properties of $(CH_3)_2NH(H_2O)_{n=1-6}$ clusters were investigated for the first time.

Small clusters with up to six water molecules exhibit slightly higher binding isotropic mean polarizabilities $\bar{\alpha}_{binding}$ in the range of −0.02–2.43 a.u., as shown in Table S2,† which is attributed to the small hydrogen-bonding network when the number of water molecules is less than 6. The isotropic mean polarizabilities $\bar{\alpha}$ are quite dependent on the number of water molecules and vary linearly, as shown in Fig. 10a, similarly to the study of methanol clusters[94] and chloride ion hydration systems,[66] and increase sharply from 47.78 to 96.86 a.u. From Fig. 10b, it is quite clearly observed that the Rayleigh scattering intensities of natural light $\mathscr{R}_n$ dramatically increase with an increase in the number of water molecules, following the trend of a second-order polynomial with correlation coefficient 0.99919. This increasing trend can be attributed to the gradually increasing isotropic mean polarizabilities $\bar{\alpha}$, which will dominate the Rayleigh scattering.

From Fig. 10c and d, the anisotropic polarizabilities $\Delta\alpha$ and depolarization ratios of natural light σ_n of $(CH_3)_2NH(H_2O)_{n=1-6}$ clusters can be observed as a function of the number of water molecules in the clusters. It is observed that the anisotropic polarizability $\Delta\alpha$ decreases from a monomer to a dimer and then increases from a dimer to a tetramer. In the case of $(CH_3)_2NH(H_2O)_{5-6}$, $\Delta\alpha$ decreases slightly then decreases by a large step from a pentamer to a hexamer. The calculated depolarization ratio of natural light σ_n has a similar variation
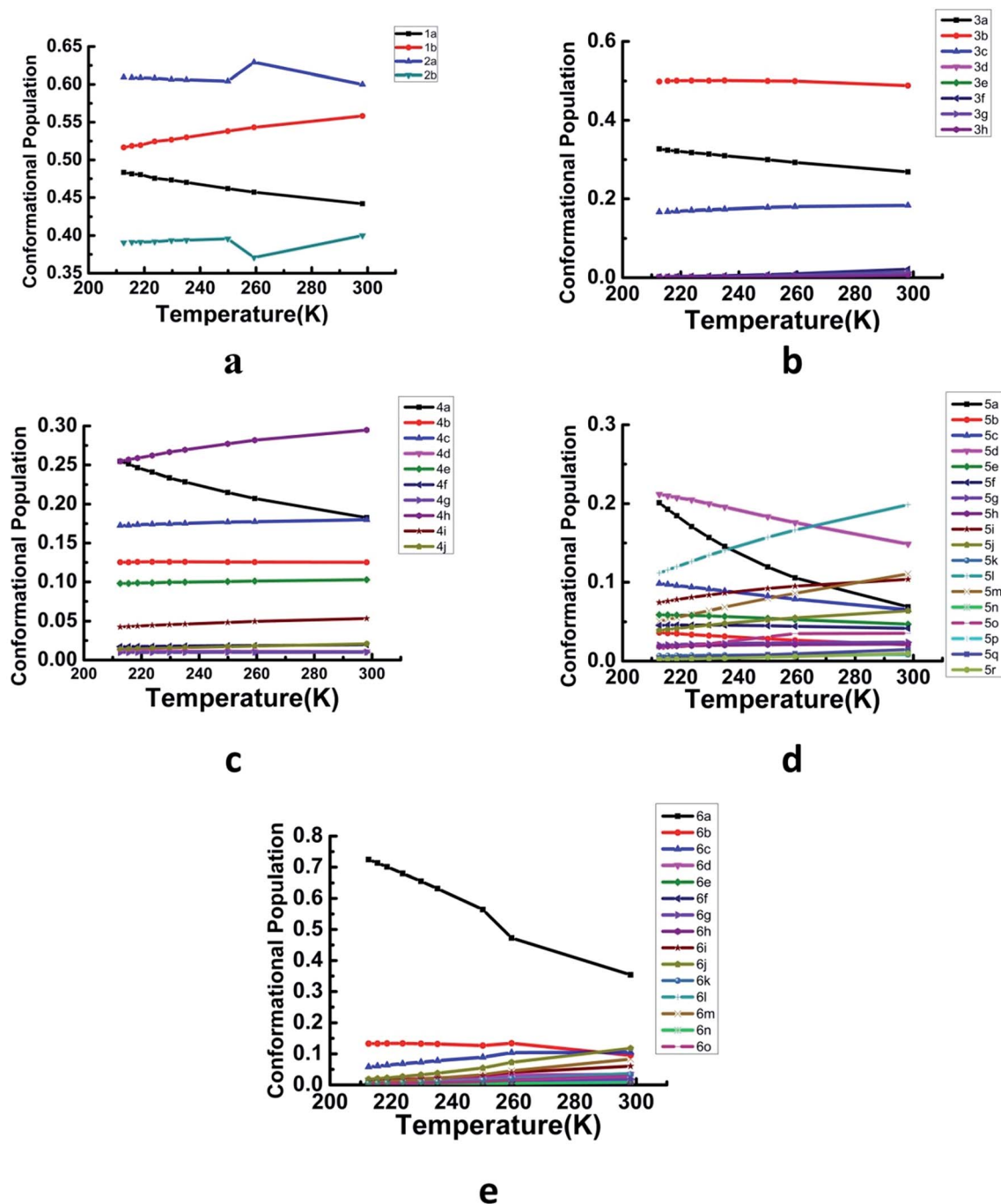
Fig. 8 Conformational population changes for the low-energy isomers of $(CH_3)_2NH(H_2O)_{1-6}$ *versus* temperature: (8a) $(CH_3)_2NH(H_2O)_{1,2}$; (8b) $(CH_3)_2NH(H_2O)_3$; (8c) $(CH_3)_2NH(H_2O)_4$; (8d) $(CH_3)_2NH(H_2O)_5$; and (8e) $(CH_3)_2NH(H_2O)_6$.

trend to the anisotropic polarizability $\Delta\alpha$, which is due to an increase in the isotropic mean polarizability $\bar{\alpha}$ in combination with the anisotropic polarizability $\Delta\alpha$; this plays the leading role and has a positive correlation with σ_n. In Fig. 2–5, it is clearly observed that clusters become quasi-planar ring structures with the addition of a second water molecule; however, the conformation changes to be a cage-like three-dimensional structure for pentamers. Therefore, this is consistent with what is to be

expected as the cluster changes from a molecular cluster into a spherical isotropic particle.

Observations by Elm *et al.*,[84] who studied the Rayleigh scattering properties of atmospheric pre-nucleation systems, found that all different conformations within each cluster yield very similar isotropic mean polarizabilities $\bar{\alpha}$ within 2 a.u. Moreover, from other studies[94,95] of Rayleigh scattering properties, remarkable differences between different conformations have been studied, which indicate that the anisotropic polarizability
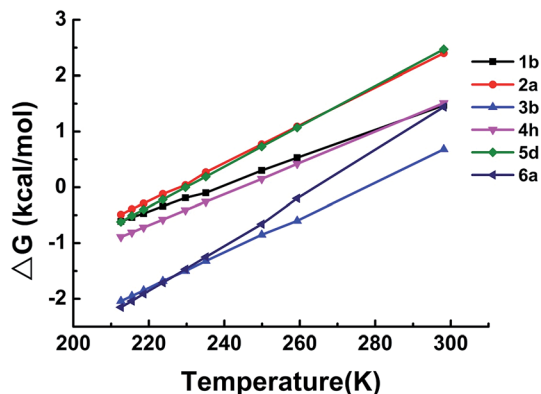
Fig. 9 Gibbs free energy changes (in kcal mol^{-1}) for the minimum thermodynamics for stepwise hydration of $(CH_3)_2NH(H_2O)_{n=1-6}$ clusters at different temperatures.

$\Delta\alpha$ and depolarization ratio σ could be alternative parameters depending on the constituents and conformations. In our study of the ten isomers of $(CH_3)_2NH(H_2O)_5$, it was observed that even though **5a**, **5c**, **5e**, **5h**, **5i**, and **5j** exhibit different hydrogen-bonding networks with various numbers of N–H and O–H

hydrogen bonds, the difference in $\bar{\alpha}_{binding}$ among these isomers is rather small, within 3 a.u., as shown in Table S2,† which is smaller for the isomers **5c**, **5d**, **5f**, and **5g** with the same bonding pattern. For the depolarization ratios of $(CH_3)_2NH(H_2O)_5$, the case is similar. Therefore, this could imply that the anisotropic polarizability and depolarization ratio cannot be regarded as alternative parameters, at least for hydrated DMA clusters, which is similar to the cases of methanol[94] and chloride ion hydration systems.[66] However, the anisotropic polarizabilities $\Delta\alpha_{binding}$ are highly isomer-dependent and fluctuate from -3.49 to 0.79 a.u. for the ten isomers of $(CH_3)_2NH(H_2O)_5$, which have been observed in sulfuric acid hydration system.[84]

4. Conclusions

We have investigated the structural evolution, non-covalent interactions, temperature effects, and optical properties of hydrated DMA clusters. The global and low-lying local minima of isomers were optimized at the PW91PW91/6-311++G(3df,3pd) level. The thermodynamics properties were further corrected using DF-MP2-F12/CBS//PW91PW91/6-311++G(3df,3pd). Electron density analysis shows that the interactions of these complexes are mainly medium hydrogen bonds, but are not
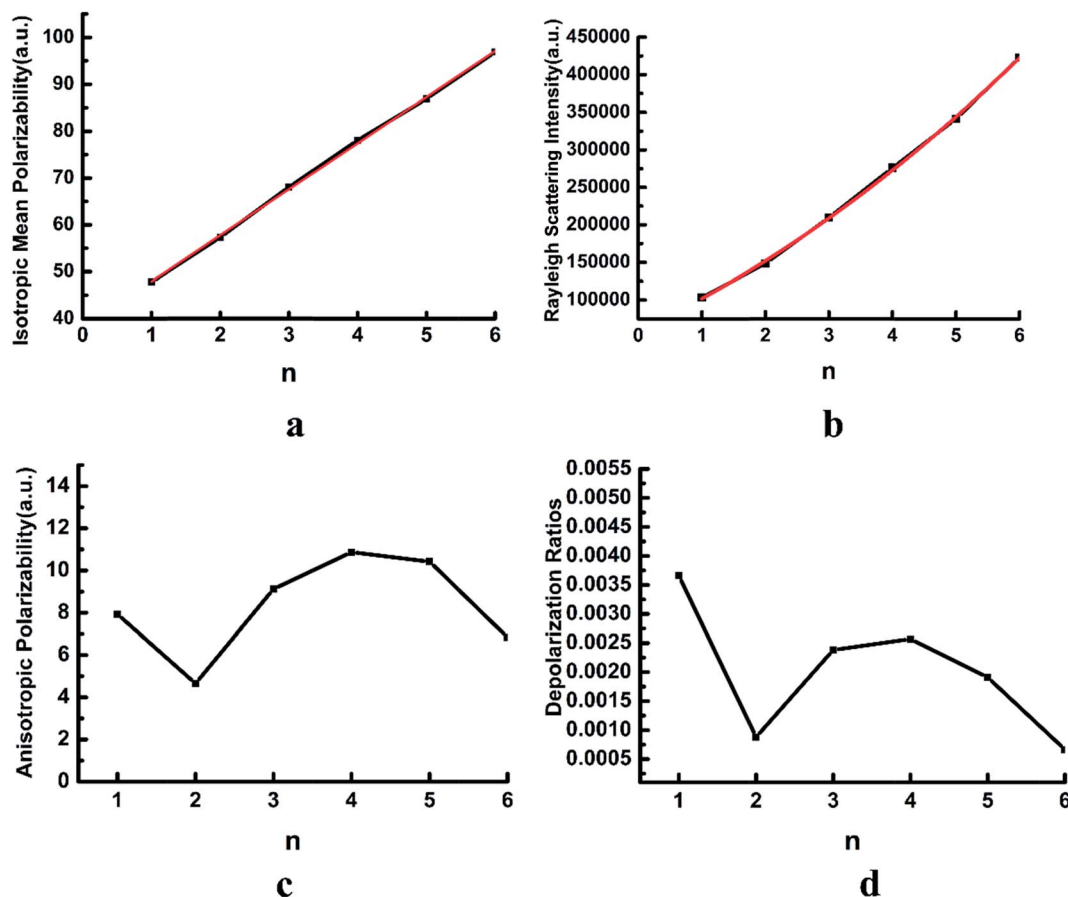

Fig. 10 Rayleigh light scattering and polarizability properties of clusters: (a) isotropic mean polarizabilities as a function of number of water molecules; (b) Rayleigh light scattering intensities as a function of number of water molecules; (c) anisotropic polarizabilities as a function of number of water molecules; (d) depolarization ratios as a function of number of water molecules.

substantial enough to overcome the energy barrier for the reaction of hydration spontaneously in the standard state of 1 atm pressure and 298 K. The dependence on temperature of the conformational population and the Gibbs free energy for the formation of $(CH_3)_2NH(H_2O)_{1-6}$ clusters were investigated. A weak dependence on temperature was found for the formation of $(CH_3)_2NH(H_2O)_{n=1-6}$ clusters. Hydrated DMA clusters are favorable with negative energy values at low temperatures, especially for $(CH_3)_2NH(H_2O)_3$, but these clusters may be difficult to form because of the combined effect of Gibbs free energies with small negative values and the low relative concentration of DMA in various atmospheric conditions. This implies that hydrated DMA clusters are difficult to form spontaneously in the atmosphere. Finally, the Rayleigh scattering properties have been investigated. It appears that the isotropic mean polarizabilities display a linear relation, whereas the Rayleigh scattering intensities of natural light follow a second-order polynomial trend as the size of the clusters increases. Furthermore, the anisotropic polarizability and depolarization ratio cannot be regarded as alternative parameters, at least for hydrated DMA clusters. Large hydrated DMA clusters need further study and this study could also provide help for the study of ternary nucleation systems containing DMA, sulfuric acid and water molecules.

Acknowledgements

References

1 R. Makkonen, A. Asmi, V.-M. Kerminen, M. Boy, A. Arneth, P. Hari and M. Kulmala, *Atmos. Chem. Phys.*, 2012, **12**, 1515–1524.

2 J. Kazil, P. Stier, K. Zhang, J. Quaas, S. Kinne, D. O'Donnell, S. Rast, M. Esch, S. Ferrachat, U. Lohmann and J. Feichter, *Atmos. Chem. Phys.*, 2010, **10**, 10733–10752.

3 M. B. Baker and T. Peter, *Nature*, 2008, **451**, 299–300.

4 M. Kulmala, H. Vehkamäki, T. Petäjä, M. Dal Maso, A. Lauri, V.-M. Kerminen, W. Birmili and P. H. McMurry, *J. Aerosol Sci.*, 2004, **35**, 143–176.

5 R. J. Charlson, J. H. Seinfeld, A. Nenes, M. Kulmala, A. Laaksonen and M. C. Facchini, *Science*, 2001, **292**, 2025–2026.

6 A. Saxon and D. Diaz-Sanchez, *Nat. Immunol.*, 2005, **6**, 223–226.

7 G. Oberdörster and M. J. Utell, *Environ. Health Perspect.*, 2002, **110**, A440.

8 P. Penttinen, K. Timonen, P. Tiittanen, A. Mirme, J. Ruuskanen and J. Pekkanen, *Eur. Respir. J.*, 2001, **17**, 428–435.

9 M. Kulmala, J. Kontkanen, H. Junninen, K. Lehtipalo, H. E. Manninen, T. Nieminen, T. Petaja, M. Sipila, S. Schobesberger, P. Rantala, A. Franchin, T. Jokinen, E. Jarvinen, M. Aijala, J. Kangasluoma, J. Hakala, P. P. Aalto, P. Paasonen, J. Mikkila, J. Vanhanen, J. Aalto, H. Hakola, U. Makkonen, T. Ruuskanen, R. L. Mauldin, J. Duplissy, H. Vehkamaki, J. Back, A. Kortelainen, I. Riipinen, T. Kurten, M. V. Johnston, J. N. Smith, M. Ehn, T. F. Mentel, K. E. J. Lehtinen, A. Laaksonen, V. M. Kerminen and D. R. Worsnop, *Science*, 2013, **339**, 943–946.

10 J. Vanhanen, J. Mikkilä, K. Lehtipalo, M. Sipilä, H. Manninen, E. Siivola, T. Petäjä and M. Kulmala, *Aerosol Sci. Technol.*, 2011, **45**, 533–542.

11 T. Petäjä, M. Sipilä, P. Paasonen, T. Nieminen, T. Kurtén, I. K. Ortega, F. Stratmann, H. Vehkamäki, T. Berndt and M. Kulmala, *Phys. Rev. Lett.*, 2011, **106**, 228302.

12 A. Hirsikko, T. Nieminen, S. Gagné, K. Lehtipalo, H. Manninen, M. Ehn, U. Horrak, V.-M. Kerminen, L. Laakso and P. McMurry, *Atmos. Chem. Phys.*, 2011, **11**, 767–798.

13 M. Sipilä, T. Berndt, T. Petäjä, D. Brus, J. Vanhanen, F. Stratmann, J. Patokoski, R. L. Mauldin, A.-P. Hyvärinen and H. Lihavainen, *Science*, 2010, **327**, 1243–1246.

14 M. Sipilä, K. Lehtipalo, M. Attoui, K. Neitola, T. Petäjä, P. Aalto, C. O'Dowd and M. Kulmala, *Aerosol Sci. Technol.*, 2009, **43**, 126–135.

15 E. Lovejoy, J. Curtius and K. Froyd, *J. Geophys. Res.: Atmos.*, 1984–2012, **2004**(109), D08204.

16 J. Kirkby, J. Curtius, J. Almeida, E. Dunne, J. Duplissy, S. Ehrhart, A. Franchin, S. Gagné, L. Ickes and A. Kürten, *Nature*, 2011, **476**, 429–433.

17 J. Zollner, W. Glasoe, B. Panta, K. Carlson, P. McMurry and D. Hanson, *Atmos. Chem. Phys.*, 2012, **12**, 4399–4411.

18 F. Yu, *Atmos. Chem. Phys.*, 2006, **6**, 5193–5211.

19 F. Yu and R. P. Turco, *Geophys. Res. Lett.*, 2000, **27**, 883–886.

20 J. Herb, Y. Xu, F. Yu and A. Nadykto, *J. Phys. Chem. A*, 2012, **117**, 133–152.

21 M. E. Erupe, A. A. Viggiano and S. H. Lee, *Atmos. Chem. Phys.*, 2011, **11**, 4767–4775.

22 D. R. Benson, J. H. Yu, A. Markovich and S. H. Lee, *Atmos. Chem. Phys.*, 2011, **11**, 4755–4766.

23 D. R. Benson, L. H. Young, F. R. Kameel and S. H. Lee, *Geophys. Res. Lett.*, 2008, **35**, L11801.

24 T. Kurtén, L. Torpo, C. G. Ding, H. Vehkamäki, M. R. Sundberg, K. Laasonen and M. Kulmala, *J. Geophys. Res.: Atmos.*, 1984–2012, **2007**(112), D04210.

25 N. Bork, J. Elm, T. Olenius and H. Vehkamäki, *Atmos. Chem. Phys.*, 2014, **14**, 12023–12030.

26 J. W. DePalma, D. J. Doren and M. V. Johnston, *J. Phys. Chem. A*, 2014, **118**, 5464–5473.

27 I. Ortega, T. Olenius, O. Kupiainen-Määttä, V. Loukonen, T. Kurtén and H. Vehkamäki, *Atmos. Chem. Phys.*, 2014, **14**, 7995–8007.

28 R. Zhang, A. Khalizov, L. Wang, M. Hu and W. Xu, *Chem. Rev.*, 2011, **112**, 1957–2011.

29 R. Zhang, *Science*, 2010, **328**, 1366–1367.

30 R. Zhang, I. Suh, J. Zhao, D. Zhang, E. C. Fortner, X. Tie, L. T. Molina and M. J. Molina, *Science*, 2004, **304**, 1487–1490.

31 J. Elm and K. V. Mikkelsen, *Chem. Phys. Lett.*, 2014, **615**, 26–29.

32 W. Xu and R. Zhang, *J. Phys. Chem. A*, 2012, **116**, 4539–4550.

33 W. Xu and R. Zhang, *J. Chem. Phys.*, 2013, **139**, 064312.

34 I. Ortega, O. Kupiainen, T. Kurtén, T. Olenius, O. Wilkman, M. McGrath, V. Loukonen and H. Vehkamäki, *Atmos. Chem. Phys.*, 2012, **12**, 225–235.

35 A. B. Nadykto, F. Yu, M. V. Jakovleva, J. Herb and Y. Xu, *Entropy*, 2011, **13**, 554–569.

36 T. Kurtén, V. Loukonen, H. Vehkamäki and M. Kulmala, *Atmos. Chem. Phys.*, 2008, **8**, 4095–4103.

37 V. Loukonen, T. Kurten, I. K. Ortega, H. Vehkamaki, A. A. H. Padua, K. Sellegri and M. Kulmala, *Atmos. Chem. Phys.*, 2010, **10**, 4961–4974.

38 J. Almeida, S. Schobesberger, A. Kürten, I. K. Ortega, O. Kupiainen-Määttä, A. P. Praplan, A. Adamov, A. Amorim, F. Bianchi and M. Breitenlechner, *Nature*, 2013, **502**, 359–363.

39 T. Berndt, F. Stratmann, M. Sipilä, J. Vanhanen, T. Petäjä, J. Mikkilä, A. Grüner, G. Spindler, L. Mauldin III and J. Curtius, *Atmos. Chem. Phys.*, 2010, **10**, 7101–7116.

40 W. Glasoe, K. Volz, B. Panta, N. Freshour, R. Bachman, D. Hanson, P. McMurry and C. Jen, *J. Geophys. Res.: Atmos.*, 2015, **120**, 1933–1950.

41 C. N. Jen, P. H. McMurry and D. R. Hanson, *J. Geophys. Res.: Atmos.*, 2014, **119**, 7502–7514.

42 M. Chen, M. Titcombe, J. Jiang, C. Jen, C. Kuang, M. L. Fischer, F. L. Eisele, J. I. Siepmann, D. R. Hanson and J. Zhao, *Proc. Natl. Acad. Sci. U. S. A.*, 2012, **109**, 18713–18718.

43 N. Freshour, K. Carlson, Y. Melka, S. Hinz, B. Panta and D. Hanson, *Atmos. Meas. Tech.*, 2014, **7**, 3611–3621.

44 D. Hanson, P. McMurry, J. Jiang, D. Tanner and L. Huey, *Environ. Sci. Technol.*, 2011, **45**, 8881–8888.

45 V. Loukonen, T. Kurtén, I. Ortega, H. Vehkamäki, A. A. Padua, K. Sellegri and M. Kulmala, *Atmos. Chem. Phys.*, 2010, **10**, 4961–4974.

46 X. Ge, A. S. Wexler and S. L. Clegg, *Atmos. Environ.*, 2011, **45**, 561–577.

47 X. Ge, A. S. Wexler and S. L. Clegg, *Atmos. Environ.*, 2011, **45**, 524–546.

48 J. Zhao, J. Smith, F. Eisele, M. Chen, C. Kuang and P. McMurry, *Atmos. Chem. Phys.*, 2011, **11**, 10823–10836.

49 H. Yu and S.-H. Lee, *Environ. Chem.*, 2012, **9**, 190–201.

50 A. B. Nadykto, J. Herb, F. Yu and Y. Xu, *Chem. Phys. Lett.*, 2014, **609**, 42–49.

51 R. F. Bader, *Chem. Rev.*, 1991, **91**, 893–928.

52 P. Paasonen, T. Olenius, O. Kupiainen, T. Kurtén, T. Petäjä, W. Birmili, A. Hamed, M. Hu, L. Huey and C. Plass-Duelmer, *Atmos. Chem. Phys.*, 2012, **12**, 9113–9133.

53 H. Henschel, J. C. A. Navarro, T. Yli-Juuti, O. Kupiainen-Määttä, T. Olenius, I. K. Ortega, S. L. Clegg, T. Kurtén, I. Riipinen and H. Vehkamaki, *J. Phys. Chem. A*, 2014, **118**, 2599–2611.

54 J. Haywood and O. Boucher, *Rev. Geophys.*, 2000, **38**, 513–543.

55 D. J. Wales and J. P. K. Doye, *J. Phys. Chem. A*, 1997, **101**, 5111–5116.

56 S. Yoo and X. C. Zeng, *J. Chem. Phys.*, 2003, **119**, 1442–1450.

57 S. H. Yoo and X. C. Zeng, *Angew. Chem., Int. Ed.*, 2005, **44**, 1491–1494.

58 W. Huang, R. Pal, L. M. Wang, X. C. Zeng and L. S. Wang, *J. Chem. Phys.*, 2010, **132**, 054305.

59 W. Huang, H. J. Zhai and L. S. Wang, *J. Am. Chem. Soc.*, 2010, **132**, 4344–4351.

60 W. Huang and L.-S. Wang, *Phys. Rev. Lett.*, 2009, **102**, 153401.

61 W. Huang, A. P. Sergeeva, H.-J. Zhai, B. B. Averkiev, L.-S. Wang and A. I. Boldyrev, *Nat. Chem.*, 2010, **2**, 202–206.

62 W. Huang, M. Ji, C.-D. Dong, X. Gu, L.-M. Wang, X. G. Gong and L.-S. Wang, *ACS Nano*, 2008, **2**, 897–904.

63 L.-L. Yan, Y.-R. Liu, T. Huang, S. Jiang, H. Wen, Y.-B. Gai, W.-J. Zhang and W. Huang, *J. Chem. Phys.*, 2013, **139**, 244312.

64 Y.-R. Liu, H. Wen, T. Huang, X.-X. Lin, Y.-B. Gai, C.-J. Hu, W.-J. Zhang and W. Huang, *J. Phys. Chem. A*, 2014, **118**, 508–516.

65 S.-S. Lv, Y.-R. Liu, T. Huang, Y.-J. Feng, S. Jiang and W. Huang, *J. Phys. Chem. A*, 2015, **119**, 3770–3779.

66 S. Jiang, T. Huang, Y.-R. Liu, K.-M. Xu, Y. Zhang, Y.-Z. Lv and W. Huang, *Phys. Chem. Chem. Phys.*, 2014, **16**, 19241–19249.

67 S. Jiang, Y. R. Liu, T. Huang, H. Wen, K. M. Xu, W. X. Zhao, W. J. Zhang and W. Huang, *J. Comput. Chem.*, 2014, **35**, 159–165.

68 S.-K. Miao, S. Jiang, J. Chen, Y. Ma, Y.-P. Zhu, Y. Wen, M.-M. Zhang and W. Huang, *RSC Adv.*, 2015, **5**, 48638–48646.

69 S.-T. Pei, S. Jiang, Y.-R. Liu, T. Huang, K.-M. Xu, H. Wen, Y.-P. Zhu and W. Huang, *J. Phys. Chem. A*, 2015, **119**, 3035–3047.

70 X.-Q. Peng, Y.-R. Liu, T. Huang, S. Jiang and W. Huang, *Phys. Chem. Chem. Phys.*, 2015, **17**, 9552–9563.

71 Y.-P. Zhu, Y.-R. Liu, T. Huang, S. Jiang, K.-M. Xu, H. Wen, W.-J. Zhang and W. Huang, *J. Phys. Chem. A*, 2014, **118**, 7959–7974.

72 B. Delley, *J. Chem. Phys.*, 1990, **92**, 508–517.

73 M. Frisch, G. Trucks, H. B. Schlegel, G. Scuseria, M. Robb, J. Cheeseman, G. Scalmani, V. Barone, B. Mennucci and G. Petersson, *Gaussian 09, revision A. 02*, Inc., Wallingford, CT, 2009, vol. 270, p. 271.

74 Y. Xu, A. B. Nadykto, F. Yu, L. Jiang and W. Wang, *J. Mol. Struct.: THEOCHEM*, 2010, **951**, 28–33.

75 J. Herb, A. B. Nadykto and F. Yu, *Chem. Phys. Lett.*, 2011, **518**, 7–14.

76 J. Elm, M. Bilde and K. V. Mikkelsen, *J. Chem. Theory Comput.*, 2012, **8**, 2071–2077.

77 W. Klopper, K. L. Bak, P. Jørgensen, J. Olsen and T. Helgaker, *J. Phys. B: At., Mol. Opt. Phys.*, 1999, **32**, R103.

78 A. Halkier, T. Helgaker, P. Jørgensen, W. Klopper, H. Koch, J. Olsen and A. K. Wilson, *Chem. Phys. Lett.*, 1998, **286**, 243–252.

79 A. Halkier, T. Helgaker, P. Jørgensen, W. Klopper and J. Olsen, *Chem. Phys. Lett.*, 1999, **302**, 437–446.

80 H. Werner, P. Knowles, G. Knizia, F. Manby, M. Schütz, P. Celani, T. Korona, R. Lindh, A. Mitrushenkov and G. Rauhut, *MOLPRO, version 2010.1*, Cardiff University, Cardiff, UK, 2010.

81 B. Temelso, T. E. Morrell, R. M. Shields, M. A. Allodi, E. K. Wood, K. N. Kirschner, T. C. Castonguay, K. A. Archer and G. C. Shields, *J. Phys. Chem. A*, 2012, **116**, 2209–2224.

82 J. G. Hill, *Int. J. Quantum Chem.*, 2013, **113**, 21–34.

83 J. R. Lane and H. G. Kjaergaard, *J. Chem. Phys.*, 2009, **131**, 034307.

84 J. Elm, P. Norman, M. Bilde and K. V. Mikkelsen, *Phys. Chem. Chem. Phys.*, 2014, **16**, 10883–10890.

85 S. Maheshwary, N. Patel, N. Sathyamurthy, A. D. Kulkarni and S. R. Gadre, *J. Phys. Chem. A*, 2001, **105**, 10525–10537.

86 E. R. Johnson, S. Keinan, P. Mori-Sanchez, J. Contreras-Garcia, A. J. Cohen and W. Yang, *J. Am. Chem. Soc.*, 2010, **132**, 6498–6506.

87 J. Contreras-García, W. Yang and E. R. Johnson, *J. Phys. Chem. A*, 2011, **115**, 12983–12990.

88 X. Yang, L. Gan, L. Han, E. Wang and J. Wang, *Angew. Chem.*, 2013, **125**, 2076–2080.

89 T. Lu and F. Chen, *J. Comput. Chem.*, 2012, **33**, 580–592.

90 W. Humphrey, A. Dalke and K. Schulten, *J. Mol. Graphics*, 1996, **14**, 33–38.

91 J. Kim, B. J. Mhin, S. J. Lee and K. S. Kim, *Chem. Phys. Lett.*, 1994, **219**, 243–246.

92 J. H. Seinfeld and S. N. Pandis, *Atmospheric chemistry and physics: from air pollution to climate change*, John Wiley & Sons Inc, Hoboken, New Jersey, 2012, pp. 691–711.

93 Y. Chan, R. Simpson, G. H. Mctainsh, P. D. Vowles, D. Cohen and G. Bailey, *Atmos. Environ.*, 1999, **33**, 3237–3250.

94 E. Orestes, P. Chaudhuri and S. Canuto, *Mol. Phys.*, 2012, **110**, 297–306.

95 P. Chaudhuri and S. Canuto, *J. Mol. Struct.: THEOCHEM*, 2006, **760**, 15–20.